THE JOURNAL OF PHYSICAL CHEMISTRY Letters

Letter

pubs.acs.org/JPCL

Computational Search for Novel Hard Chromium-Based Materials

Alexander G. Kvashnin,*[†,‡] Artem R. Oganov,[†,‡,§,∥] Artem I. Samtsevich,[†] and Zahed Allahyari[†,‡]

[†]Skolkovo Institute of Science and Technology, Skolkovo Innovation Center, 3 Nobel Street, Moscow 143026, Russian Federation

[‡]Moscow Institute of Physics and Technology, 9 Institutsky Lane, Dolgoprudny 141700, Russian Federation

[§]Department of Geosciences and Center for Materials by Design, Institute for Advanced Computational Science, State University of New York, Stony Brook, New York 11794-2100, United States

[∥]International Center for Materials Design, Northwestern Polytechnical University, Xi'an 710072, China

Supporting Information

ABSTRACT: Nitrides, carbides, and borides of transition metals are an attractive class of hard materials. Our recent preliminary explorations of the binary chemical compounds indicated that chromium-based materials are among the hardest transition metal compounds. Motivated by this, here we explore in detail the binary Cr−B, Cr−C, and Cr−N systems using global optimization techniques. Calculated enthalpy of formation and hardness of predicted materials were used for Pareto optimization to define the hardest materials with the lowest energy. Our calculations recover all numerous known stable compounds (except $Cr_{23}C_6$ with its large unit cell) and discover a novel stable phase $Pmn2_1$-Cr_2C. We resolve the structure of Cr_2N and find it to be of anti-$CaCl_2$ type (space group *Pnnm*). Many of these phases possess remarkable hardness, but only CrB_4 is superhard (Vickers hardness 48 GPa). Among chromium compounds, borides generally possess the highest hardnesses and greatest stability. Under pressure, we predict stabilization of a layered TMDC-like phase of Cr_2N, a WC-type phase of CrN, and a new compound CrN_4. Nitrogen-rich chromium nitride CrN_4 is a high-energy-density material featuring polymeric nitrogen chains. In the presence of metal atoms (e.g., Cr), polymerization of nitrogen takes place at much lower pressures; CrN_4 becomes stable at ∼15 GPa (cf. 110 GPa for synthesis of pure polymeric nitrogen).

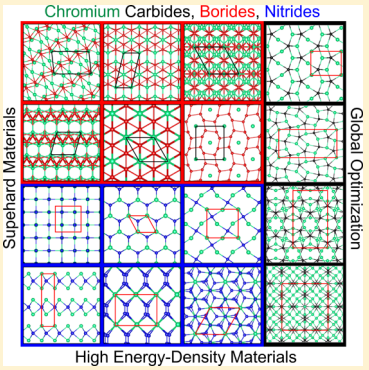

Generally, the hardest and most popular superhard materials known to date belong to two groups, (1) some B−C−N compounds and their derivatives (e.g., refs 1 and 2) and (2) nitrides, carbides, and borides of some transition metals. Compounds of the first class are semiconducting and brittle, and the best-known superhard phases (i.e., with Vickers hardness > 40 GPa) belong to it, whereas those of the second class are usually metallic and more ductile. These two classes of very hard materials were uncovered in our preliminary computational searches across the chemical space. We explore a number of combinations of these elements, searching for materials with the best property (e.g., highest hardness, computed using the Lyakhov−Oganov model[3]). We indeed found diamond to be the hardest possible single-crystal material and B−C−N phases to have the highest hardnesses, and among non-B−C−N compounds, the Cr−B, Cr−C, and Cr−N systems were indicated among the most promising for the existence of new hard and superhard materials. Indeed, recent theoretical studies of chromium nitrides and borides reported that CrB_4 and hypothetical metastable CrN_2 can have hardnesses of 47[4,5] and 46 GPa,[6] respectively.

Usually, chromium metal and its compounds are used in a wide range of applications mainly related to wear-resistant coatings,[7−12] cutting tools,[13,14] and metal forming and plastic molding applications.[15] Chromium nitride, CrN, is often used in medical implants and tools as a coating material due to its good wear, oxidation, and corrosion resistance.[9−11] CrN is also a valuable component in advanced multicomponent coating systems, such as CrAlN, for hard, wear-resistant applications on cutting tools.[16]

Experimentally, six different chromium borides (Cr_2B, Cr_5B_3, CrB, Cr_3B_4, CrB_2, and CrB_4) are known,[17−21,4] and recently, their mechanical characteristics were examined theoretically.[4,5,22] The experimental Vickers hardness of most Cr−B phases ranges from 20.7 to 24 GPa,[23,24] while the Vickers hardness of the CrB_4 phase was reported to be in the range 29−44 GPa.[24]

It is known from experiments that there are three stable chromium carbides, $Cr_{23}C_6$, Cr_3C_2, and Cr_7C_3.[12−14,25,26] Powders of Cr_3C_2 were prepared by heat treatment of metastable chromium oxides of controlled morphology in a H_2−CH_4 atmosphere.[8] Other metastable chromium carbides such as CrC and Cr_3C have also been synthesized.[27−30] Theoretically calculated values of Vickers hardness of chromium carbide phases by the Šimůnek model[31] vary from 13 to 32 GPa,[32] which is in good agreement with experiments.[33−35]

Received: December 2, 2016
Accepted: January 19, 2017
Published: January 20, 2017

DOI: 10.1021/acs.jpclett.6b02821
J. Phys. Chem. Lett. 2017, 8, 755−764

Table 1. Lattice Parameters of Predicted Cr−B and Cr−C Phases

comp.	space group	lattice parameters, Å	V, Å^3/unit	ρ, g/cm^3
Cr_2B	$I4/m$	a = 4.21, b = 6.59, c = 4.04	27.95	6.82
Cr_5B_3	$I4/mcm$	a = 5.43, b = 2.66, c = 4.56	73.15	6.64
CrB	$Cmcm$	a = 2.92, b = 7.84, c = 2.92 (theor: a = 2.93, b = 7.84, c = 2.92)[21] (exp: a = 2.959, b = 7.846, c = 2.919)[21]	66.79	6.25
Cr_3B_4	$Immm$	a = b = 2.92, c = 6.54	55.82	5.93
CrB_4	$Pnnm$	a = 5.47, b = 2.85, c = 4.72 (exp: a = 5.48, b = 2.87, c = 4.74)[4,24] (exp: a = 5.48, b = 2.87, c = 4.75)[20]	36.85	4.29
CrB_2	$P6/mmm$	a = b = 2.98, c = 2.91 (theor: a = b = 2.97, c = 3.08)[55] (exp: a = b = 2.97, c = 3.07)[17,24]	22.46	5.44
Cr_7C_3	$Pnma$	a = 4.48, b = 6.94, c = 12.01 (theor: a = 4.51, b = 6.91, c = 12.08)[32] (exp: a = 4.53, b = 7.01, c = 12.14)[56]	93.46	7.11
Cr_2C	$Pmn2_1$	a = 5.01, b = 2.82, c = 3.98	28.13	6.85
Cr_3C_2	$Pnma$	a = 2.78, b = 5.47, c = 11.45 (theor: a = 2.79, b = 5.48, c = 11.47)[32] (exp: a = 2.83, b = 5.55, c = 11.49)[57]	43.72	6.84
$Cr_{23}C_6$	$Fm\bar{3}m$	a = b = c = 10.82 (theor: a = b = c = 10.56)[32] (exp: a = b = c = 10.66)[58]	291.04	7.09

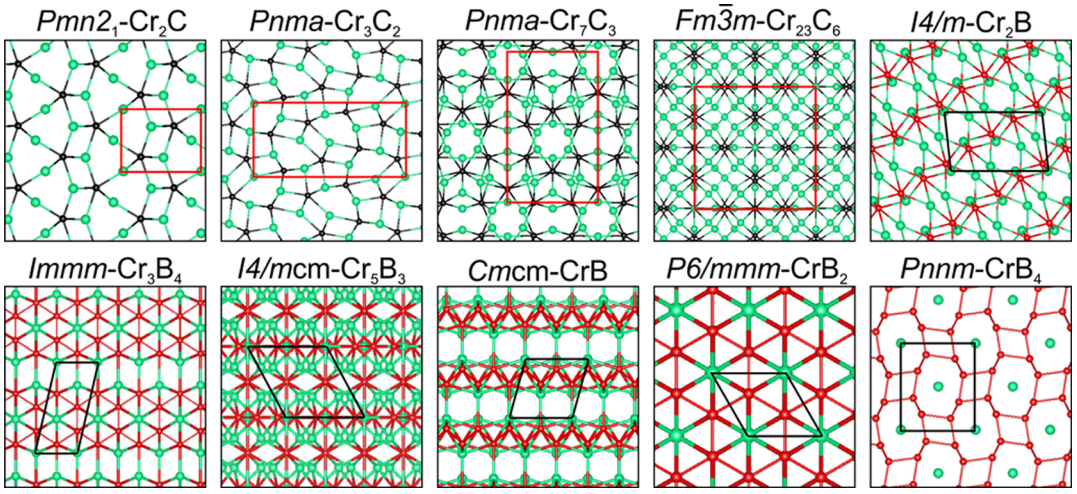

Figure 1. Crystal structures of predicted Cr−C and Cr−B phases. Cr atoms are green, carbon is black, and boron is red.

Chromium nitrides are less studied, with most experimental works devoted to CrN and reporting the existence of a cubic paramagnetic B1 phase (NaCl-type) with $Fm\bar{3}m$ space group.[36,37] However, at temperatures below the Néel temperature (200−287 K),[37−40] the B1-CrN phase transforms to an orthorhombic antiferromagnetic phase with *Pnma* space group,[37,39] and this transition was studied theoretically.[41] Today, electronic and magnetic properties of chromium nitride at low temperatures are actively studied.[37,41−44]

In addition to CrN, there is another stable compound Cr_2N, which appears together with CrN during the fabrication of Cr−N films and displays comparable wear resistance but worse oxidation resistance.[45−48] Coating of Cr_2N can be synthesized by either solid-state metathesis reaction of $CrCl_3$ with Li_3N[49] or by controlling the N flux.[47,48,50−52] The theoretically predicted crystal structure of Cr_2N[53] was based on experimental data of Eriksson,[50] which reported a hexagonal close-packed structure with a $P\bar{3}1m$ space group with lattice parameters of a = 4.752 Å and c = 4.429 Å. Recently, comprehensive first-principles calculations of the atomic structure and physical properties of different Cr_2N phases with only varying distribution of the N atoms were reported.[54]

It is important that none of the above-mentioned works attempted global optimization of Cr−B, Cr−C, and Cr−N systems and considered only already known or hypothesized compounds.

In this Letter, we explore the Cr−B, Cr−C, and Cr−N systems using the evolutionary structure prediction algorithm USPEX and density functional theory (DFT). The structure, stability, elastic constants, and hardness of all considered phases are studied in detail.

First, we searched for stable compounds in the Cr−B, Cr−C, and Cr−N systems at zero pressure. On the basis of the calculated enthalpies of formation of predicted phases for different compositions, convex hull diagrams were constructed, shown in Figure 2a−c. Red points in the convex hull diagrams correspond to thermodynamically stable phases (see Figure 2a−c), and open points are studied metastable phases (see Figure 2c,f). One can note from Figure 2a that five chromium borides were found including $I4/m$-Cr_2B, $I4/mcm$-Cr_5B_3, $Cmcm$-CrB, $Immm$-Cr_3B_4, $P6/mmm$-CrB_2, and $Pnnm$-CrB_4. All of these predicted phases were already known from previous experimental works[18,19,24] and are successfully found here in an unbiased calculation.

During an evolutionary search of the Cr−C system, we found only three thermodynamically stable phases of chromium carbides, shown in Figure 2b by red points: *Pnma*-Cr_7C_3, $Pmn2_1$-Cr_2C, and *Pnma*-Cr_3C_2. However, there is one stable phase $Cr_{23}C_6$ with $Fm\bar{3}m$ space group, which has not been found due to a large number of atoms (29) in the unit cell (blue point in Figure 2b). The crystal structure of $Fm\bar{3}m$-$Cr_{23}C_6$ was taken from experiment,[32] and the formation enthalpy was calculated to compare it with found structures. Our calculations confirm stability of all the experimentally known chromium carbides and predict stability of a hitherto unknown phase $Pmn2_1$-Cr_2C.[8,25] In the Cr−N system, only two thermodynamically stable phases were found: *Pnma*-CrN and *Pnnm*-Cr_2N. These phases were experimentally synthesized in a number of studies,[36,37,47−52] although the structure of Cr_2N

DOI: 10.1021/acs.jpclett.6b02821
J. Phys. Chem. Lett. 2017, 8, 755−764

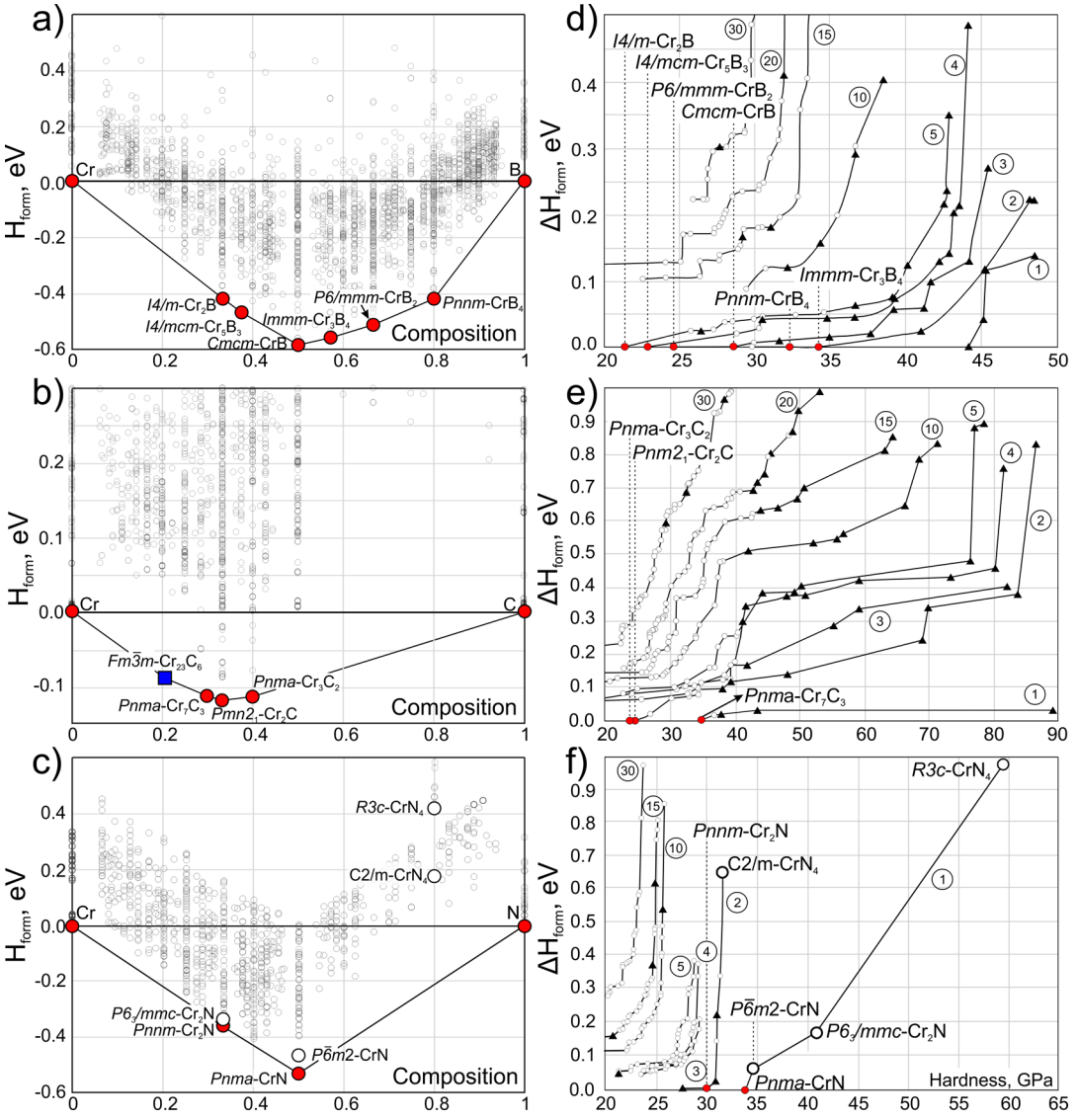

Figure 2. Convex hull diagrams of (a) Cr−B, (b) Cr−C, and (c) Cr−N systems and results of Pareto optimization in terms of formation enthalpies and hardness, computed using the Lyakhov−Oganov model[3] for (d) Cr−B, (e) Cr−C, and (f) Cr−N systems. Numbers in circles denote the number of the Pareto front. Full circles are stable phases, open circles are metastable binary phases, and full triangles are one-component phases. The square is the $Fm\bar{3}m$−$Cr_{23}C_6$ structure from ref 32.

remained unknown. Other predicted phases, denoted by green points, are metastable (see Figure 2c). Structural parameters of all predicted phases are summarized in Table 1 and illustrated in Figure 1.

Let us now consider results of Pareto optimization shown in Figure 2d−f. All points, which belong to a certain Pareto front, are connected by a black line. The first Pareto front contains phases with simultaneously optimal high hardness (estimated using Lyakhov−Oganov model[3]) and maximum stability (measured as the vertical distance from the convex hull). We consider the most promising phases, which are located mostly in the first five Pareto fronts, shown by red and open circles, which lie on the convex hull or close to it (see Figure 2d−f). We note that the Lyakhov−Oganov model, convenient, numerically stable, and usually reliable, was used for Pareto screening (and shown in Figure 2); however, it must be noted that Chen's model[59] is more accurate (these values are given in Table 2 and taken as final theoretical hardnesses in this work).

The most remarkable hardnesses, as well as the largest negative enthalpies of formation, are seen in the Cr−B system. CrB_4 is predicted to be superhard (H_v = 47.6 GPa), while all of the other stable Cr−B phases display hardnesses below 35 GPa (see Table 2), which agrees well with reference experimental data.[23,24] Other phases with higher hardness have higher formation enthalpy and therefore are metastable or unstable at zero pressure. Most structures with hardness > 40 GPa are pure boron phases. Predicted stable Cr−C phases have a Vickers hardness below 22 GPa (see Table 2), in agreement with experimental observations.[33−35] Phases with hardnesses of about 70−80 GPa are hypothetical metastable carbon allotropes, and the hardest phase in the first Pareto front (Figure 2e) with a hardness of 89 GPa is diamond with a formation enthalpy of 0.028 eV/atom, which agrees well with reference data.[60,61]

Results of Pareto optimization of the Cr−N system show that thermodynamically stable CrN and Cr_2N phases display hardnesses up to 30 GPa. While metastable CrN_2 is predicted

DOI: 10.1021/acs.jpclett.6b02821
J. Phys. Chem. Lett. 2017, 8, 755−764

Table 2. Mechanical Properties of Chromium-Based Materials, Including the Bulk Modulus (B), Shear Modulus (G), Hardness Calculated Using Gao's Model (H_G), Chen's Model (H_C), and the Lyakhov–Oganov Model (H_{LO}), Pugh's Modulus Ratio ($k = G/B$), and Thermal Expansion for Cr–N Phases at 300 K (α)

comp.	space group	B, GPa	G, GPa	H_G, GPa	H_C, GPa	H_{LO}, GPa	k	α, 10^{-6} K^{-1}
Cr_2B	$I4/m$	269.5	178.3	28.1	22.6	21.5	0.66	–
Cr_5B_3	$I4/mcm$	250.7	189.4	26.2	27.9	22.9	0.76	–
CrB	$Cmcm$	255.3 (theor: 304.8)[21] (exp: 269)[21]	209.5 (theor: 225.4)[21]	32.6 (exp: 19.2–23)[21,23]	33.2	28.6	0.82	–
Cr_3B_4	$Immm$	276.6	202.8	32.9 (exp: 20.9–23.0)[23]	28.1	34.1	0.73	–
CrB_4	$Pnnm$	252.6 (theor: 265)[4] (exp: 232)[24]	251.8 (theor: 267[22]) (exp: 261[4])	36.6 (theor: 46.8)[5] (exp: 28.6–44)[24]	47.6 (theor: 48)[4]	32.9	0.83	–
CrB_2	$P6/mmm$	278.4 (theor: 298)[5] (exp: 228)[24]	156.4 (theor: 172)[5]	23.6 (exp: 23.1–15.8)[24]	16.6	24.8	0.56	–
Cr_7C_3	$Pnma$	264.6 (theor: 300.6)[32]	104.4 (theor: 118)[32]	25.1 (theor: 18.3[32])	7.2 (exp: 16.9,[34] 17,[63] 16[35])	33.1	0.44	–
Cr_2C	$Pmn2_1$	292.8	184.5	27.3	21.6	24.5	0.63	–
Cr_3C_2	$Pnma$	296.2 (theor: 312.9)[32]	163.6 (theor: 162)[56]	26.6 (theor: 20.9[32])	16.7 (exp: 18.9,[63] 18.3[64])	31.5	0.55	–
$Cr_{23}C_6$ ref.[32]	$Fm\bar{3}m$	263.4 (theor: 282.3)[32] (exp: 300)[56]	178.3	24.8 (theor: 13.2,[32] exp: 15[63])	14.1	21.5	0.53	–
CrN ($U-J$ = 1 eV)	$Pnma$	221.4 (exp: 262)[39]	152.1	35.8	21.4	34.8	0.72	2.01
CrN ($U-J$ = 1 eV)	$P\bar{6}m2$	312.6	220.5	36.8	28.2	34.6	0.74	2.14
Cr_2N	$Pnnm$	235.4	133.1	31.8	15.0	31.3	0.59	2.05
Cr_2N	$P6_3/mmc$	239.8	116.1	37.9	11.0	41.0	0.47	2.55
CrN_4 ($U-J$ = 1 eV)	$C2/m$	26.7	21.8	46.8	2.2	31.6	0.82	6.52
CrN_4 ($U-J$ = 1 eV)	$R3c$	176.6	101.1	57.2	12.5	59.5	0.59	1.39
CrN_2 ref 6	$P\bar{6}m2$	273.6 (theor: 366)[6]	235.3 (theor: 256)[6]	46.3 (theor: 45.9)[6]	29.5	44.4	0.69	–

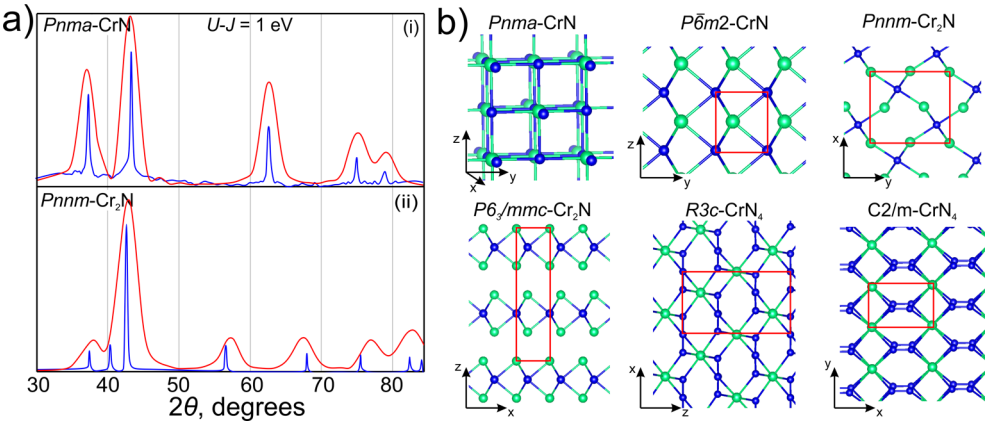

Figure 3. (a) Simulated XRD pattern with λ = 1.54 Å. Blue lines are experimental XRD patterns from ref 49. (b) Crystal structures of CrN, Cr_2N, and CrN_4 phases. Green spheres, Cr atoms; blue, N atoms.

to be superhard using Gao's and Lyakhov–Oganov models, Chen's model gives a lower hardness (29.5 GPa). For metastable CrN_4 structures located in the first and second Pareto fronts (open circles in Figure 2f), the predicted Lyakhov–Oganov hardness of ~60 GPa is a rare failing of this model; the more accurate Chen's model predicts much lower values (see Table 2). For the other phases, agreement between different models of hardness is much better. We also calculated the ideal strength of *Pnma*-CrN, *P*$\bar{6}$*m2*-CrN, *Pnnm*-Cr_2N, *R3c*-CrN_4, and *Pnnm*-CrB_4 phases to be equal to 38.2, 41.7, 37.3, 24.2, and 52.5 GPa, respectively. The ideal strength of *Pnnm*-CrB_4 was calculated before,[22] in close agreement with our result. Obtained values of ideal strength correspond well with data for Vickers hardness calculated by Chen's model.

We examined the mechanical properties of considered phases, summarized in Table 2. Considering the Cr–B system, the maximum value of the bulk modulus was obtained for the *P6/mmm*-CrB_2 phase (278 GPa). The *Pnnm*-CrB_4 phase displays the largest value of shear modulus (252 GPa), which agrees extremely well with the theoretical and experimental values (267[22] and 261 GPa,[4] respectively). Among chromium carbides, the highest bulk modulus is 296 GPa for *Pnma*-Cr_3C_2,

DOI: 10.1021/acs.jpclett.6b02821
J. Phys. Chem. Lett. 2017, 8, 755–764

and the highest shear modulus is 292 GPa for the $Pmn2_1$-Cr_2C phase. The highest bulk modulus of Cr−N phases corresponds to the $P\bar{6}m2$-CrN phase (312 GPa). It was expected that this tungsten carbide (WC-type) phase would reveal exceptional mechanical properties (WC has a bulk modulus of 439 GPa[62]). The bulk moduli of *Pnnm* and $P6_3/mmc$ phases of Cr_2N are 232 and 239 GPa, respectively. More detailed information on the elastic tensors of the studied phases is summarized in Table S2 (Supporting Information).

We paid more attention to the less studied Cr−N system and its stable and metastable phases. Part of the interest in new nitride phases comes from the possibility of reduction of the pressure of nitrogen polymerization for synthesis of high-energy-density materials. It is necessary to compress pure nitrogen to >110 GPa[65] to obtain a polymeric phase, and such a high pressure precludes any practical applications. One of the possible ways to reduce the polymerization pressure is to combine nitrogen with metal ions (such as chromium, explored here). Indeed, it was found previously that presence of sodium reduces the polymerization pressure of nitrogen down to ∼80 GPa in the compound NaN_3.[66]

In the convex hull diagram of the Cr−N system, three different compositions of CrN_x were found with x = 0.5, 1, and 4. The X-ray diffraction (XRD) patterns are shown in Figure 3a. One can see good agreement between simulated and experimental[49] XRD patterns of *Pnma*-CrN, shown in the (i) panel of Figure 3a. We found that the XRD pattern of the predicted *Pnnm*-Cr_2N agrees perfectly with experimental data from ref 49 (see Figure 3a, panel (ii)). This phase, observed in several experimental works,[47−52] remained structurally unresolved until now, but here we finally determine its crystal structure; it has the *Pnnm* space group and is isostructural with calcium chloride ($CaCl_2$)[67] and poststishovite SiO_2[68] (see Figure 3b).

The *Pnma*-CrN phase has a NaCl-type structure with orthorhombic distortion due to antiferromagnetic ordering, while predicted $P\bar{6}m2$-CrN is isostructural with WC. Another phase of Cr_2N with space group $P6_3/mmc$ has a layered structure and is isostructural to layered transition metal dichalcogenides (TMDCs), shown in Figure 3b. This phase could be considered as a possible material for isolation of a single layer of Cr_2N using micromechanical cleavage.[69,70] Newly predicted CrN_4 is found in two forms, with space groups $R3c$ and $C2/m$; their structures are shown in Figure 3b. Detailed structural parameters and energies relative to the convex hull (see Figure 2c) of considered phases are summarized in Table 3.

Computed phonon densities of states for the *Pnma* and $P\bar{6}m2$ CrN phases at zero pressure are shown in the (i) panel of Figure 4a and display the absence of imaginary phonon frequencies, which manifests the dynamical stability of both CrN phases. The phase transition pathway from *Pnma* to $P\bar{6}m2$ CrN was modeled by the variable-cell nudged elastic band (VCNEB) method[71] and is shown in Figure S1 (see the Supporting Information for details).

Both of the Cr_2N phases (with space groups *Pnnm* and $P6_3/mmc$) were found to be dynamically stable (see panel (ii) of Figure 4a), the formed being energetically slightly more stable and matching perfectly the experimental XRD patterns (Figure 3a). It is important to note that for metallic Cr_2N phases we did not use the Hubbard U-term correction, in contrast to CrN and CrN_4 phases. Detailed information on the choice of the $U-J$ parameter is described in the Supporting Information.

Table 3. Structural Parameters of Cr−N Phases

comp.	lattice parameters, Å	V, Å^3/unit	ρ, g/cm^3		positions			ΔH_{form}, eV
Pnma CrN ($U-J$ = 1 eV)	$a = c$ = 4.19, b = 4.17 (exp: cubic CrN a = 4.148,[37] a = 4.151,[39] *ortho*-CrN a = 4.151, c = 4.082[39])	18.33	5.97	Cr	0.0	0.0	0.0	0.0
				N	1/2	1/2	1/2	
$P\bar{6}m2$ CrN ($U-J$ = 1 eV)	$a = b$ = 2.67, c = 2.59	16.05	6.82	Cr	0.0	0.0	0.0	0.066
				N	1/3	2/3	1/2	
Pnnm Cr_2N	a = 4.79, b = 4.33, c = 2.79	29.12	7.53	Cr	0.164	0.242	0.0	0.0
				N	0.0	1/2	1/2	
$P6_3/mmc$ Cr_2N	$a = b$ = 2.67, c = 9.19	28.29	6.93	Cr	0.0	−0.172	−0.112	0.005
				N	0.0	−0.162	1/4	
$C2/m$ CrN_4 ($U-J$ = 1 eV)	a = 7.64, b = 7.45, c = 3.91	44.41	3.32	Cr	0.0	0.0	0.0	0.364
				Cr	0.0	1/2	0.0	
				N	1/2	0.28	−0.349	
				N	0.285	0.0	0.371	
				N	−0.279	0.0	0.328	
$R3c$ CrN_4 ($U-J$ = 1 eV)	$a = b$ = 4.56, c = 13.81	49.74	4.18	Cr	0.0	0.0	−0.157	0.689
				N	0.339	0.376	1/4	
				N	0.0	0.0	−0.421	
$P\bar{6}m2$ CrN_2 ref 6	$a = b$ = 2.68, c = 3.67 ($U-J$ = 1 eV) ($a = b$ = 2.72, c = 3.71, $U-J$ = 3 eV)[6]	22.76 (23.86)[6]	4.24	Cr	0.0	0.0	0.0	0.055
				N	2/3	1/3	0.682	

DOI: 10.1021/acs.jpclett.6b02821
J. Phys. Chem. Lett. 2017, 8, 755−764

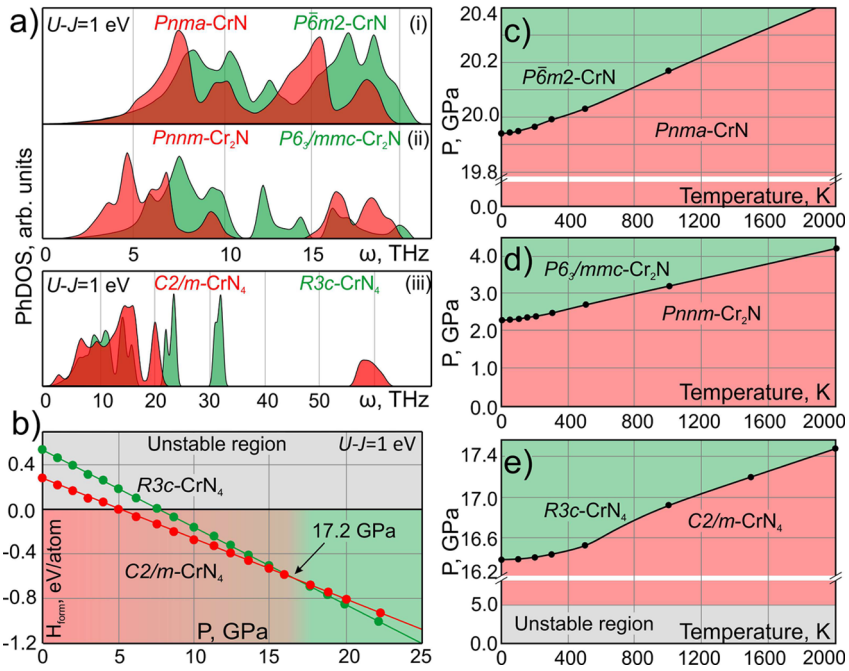

Figure 4. (a) Phonon densities of states of Cr−N phases. (b) Dependence of the enthalpy of formation on the external pressure for CrN_4 phases. Phase diagrams of (c) CrN, (d) Cr_2N, and (e) CrN_4.

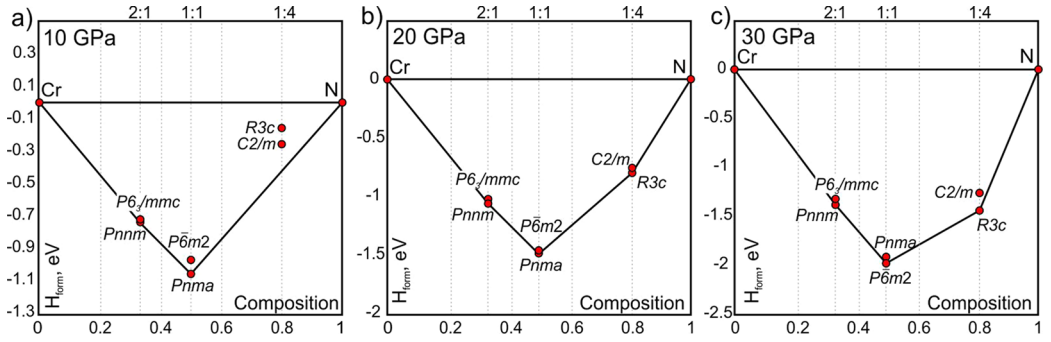

Figure 5. Convex hull diagrams for Cr−N system at (a) 10, (b) 20, (c) 30 GPa.

Two lowest-enthalpy CrN_4 phases that emerged from our evolutional searches are in fact high-energy-density materials with polymeric nitrogen chains with two atoms ($C2/m$-CrN_4) and flat triangle groups of N_4, similar to NO_3 groups but with the oxygen atoms substituted by nitrogen atoms ($R3c$-CrN_4) in the repeat unit. The effect of electron correlation is important in these phases; for example, they are both dynamically unstable at $U-J = 0$ eV (see Figure S2) and dynamically stable with $U-J = 1$ eV (see Figure 4a, panel (iii)).

Both CrN_4 phases are metastable at zero pressure and even have positive enthalpies of formation (see Figure 2c). However, at pressures above 5 GPa, the formation enthalpy of the $C2/m$ phase becomes negative (above 7.5 GPa for $R3c$-CrN_4), and at a pressure of 17 GPa, the phase transition $C2/m \rightarrow R3c$ occurs. Calculations of the phase transition pressure with $U-J$ from 0 to 5 eV gave the phase transition pressure in a region from 12 to 24 GPa at 0 K. At pressures above ∼15 GPa, CrN_4 becomes thermodynamically stable (see Figure 5).

Containing polymeric nitrogen chains, at normal conditions CrN_4 can be a high-energy-density material. We estimated the energy density of CrN_4 (equal to the enthalpy of reaction $CrN_4 \rightarrow CrN + 3/2N_2$) to be equal to 1.96 and 3.51 MJ/kg for $C2/m$ and $R3c$ phases, respectively. For comparison, the energy density of TNT (trinitrotoluene) is 4.6 MJ/kg,[72] for gun powder, it is 3 MJ/kg, for nitroglycerin, it is 6.6 MJ/kg,[73] and for lead azide, it is 2.6 MJ/kg.[74] Our results show that the presence of metals (such as Cr) lowers the pressure of polymerization of nitrogen even though with reduced (but still high) energy density.

Conditions for experimental synthesis of CrN phases were estimated by computing phase diagrams, shown in Figure 4c, where the $Pnma \rightarrow P\bar{6}m2$ phase transition pressure at 0 K is 19.9 GPa, which is readily achievable in experiments. The phase boundary between $Pnnm$ and $P6_3/mmc$ phases of Cr_2N is shown in Figure 4d, where the $Pnnm$ phase undergoes phase transition to $P6_3/mmc$ at 2.2 GPa at 0 K. Thus, it should be possible to synthesize a new Cr_2N phase with a layered structure at very mild pressures, and this phase should remain dynamically stable upon decompression to ambient pressure. The computed phase diagram of the pressure-induced $C2/m \rightarrow R3c$ phase transition of CrN_4 is shown in Figure 4 e, where the phase transition pressure is 16.4 GPa at 0 K.

The convex hull diagrams of Cr−N phases were calculated at pressures of 10, 20, and 30 GPa, as shown in Figure 5. We see the same stable compositions as at zero pressure, and in

DOI: 10.1021/acs.jpclett.6b02821
J. Phys. Chem. Lett. 2017, 8, 755−764

addition, CrN_4 becomes thermodynamically stable at pressures above ~15 GPa.

To conclude: in this work, we studied new phases in the Cr−B, Cr−C, and Cr−N systems using global optimization combined with the Pareto optimization technique, which allows us to search for new stable materials with outstanding hardness. We found all experimentally known chromium borides, carbides, and nitrides (except $Cr_{23}C_6$ with a relatively large unit cell) and predicted several new phases. The hardness of the predicted phases was calculated using different models and compared with available experimental and theoretical data. Overall, chromium borides are shown to possess the highest hardnesses and largest negative enthalpies of formation, compared to carbides and nitrides. The only thermodynamically stable superhard compound here is CrB_4 with a predicted hardness of ~48 GPa, in excellent agreement with experiments.[24] Detailed investigation of the less studied Cr−N system was carried out. The previously unresolved crystal structure of Cr_2N was shown to be of anti-$CaCl_2$ type (space group *Pnnm*). We found that synthesis of CrN_4 phases with an energy density up to 3 MJ/kg and featuring polymeric nitrogen chains can be realized by applying pressure above ~15 GPa, much lower than the 110 GPa needed to synthesize pure polymeric nitrogen.

Methods used in this study: stable phases in the Cr−B, Cr−C, and Cr−N systems were predicted using a first-principles variable-composition evolutionary algorithm (EA) in coupling with the Pareto optimization technique as implemented in the USPEX code.[75−80] Here, evolutionary searches were combined with structure relaxations using DFT[81,82] within the spin-polarized generalized gradient approximation (Perdew−Burke−Ernzerhof functional),[83] as implemented in the VASP[84−86] package. The plane-wave energy cutoff was set to 500 eV. To study the phase transition pathways of CrN phases, we used the VCNEB[71] method as implemented in the USPEX code. In order to take into account strong electron correlations between the localized 3d electrons of Cr atoms, the GGA+*U* approach within Dudarev's formulation[87,88] was applied in some cases (unless explicitly stated otherwise, $U-J = 0$ was used). For Brillouin zone sampling, Γ-centered *k*-meshes of $2\pi \times 0.05$ Å^{-1} resolution were used, ensuring excellent convergence of total energies. During structure searches, the first generation was produced randomly within 16 atoms in the unit cell, and succeeding generations were obtained by applying heredity (40%), softmutation (20%), and transmutation (20%) operations, respectively, and 20% of each generation was produced using a random symmetry structure generator. Two types of variable-composition calculations were performed in each binary system (Cr−B, Cr−C, Cr−N): (1) optimizing stability and (2) jointly optimizing stability and hardness with Pareto ranking of all structures (in the latter case, the fitness of each structure was taken to be equal to the order of its Pareto front).

For the predicted crystal structures, we performed high-quality calculations of their physical properties. Crystal structures were relaxed until the maximum net force on atoms became less than 0.01 eV/Å. The Monkhorst−Pack scheme[89] was used to sample the Brillouin zone, using 12 × 12 × 12 (*Pnma*-CrN), 8 × 8 × 10 (*Pnnm*-Cr_2N), 12 × 12 × 8 (*C*2/*m*-CrN_4), 6 × 6 × 6 ($Fm\bar{3}m$-$Cr_{23}C_6$), 8 × 8 × 8 ($Pmn2_1$-Cr_2C), 8 × 6 × 4 (*Pnma*-Cr_3C_2), 8 × 6 × 4 (*Pnma*-Cr_7C_3), 8 × 8 × 8 (*I*4/*m*-Cr_2B), 8 × 8 × 6 (*Immm*-Cr_3B_4), 8 × 8 × 6 (*I*4/*mcm*-Cr_5B_3), 8 × 8 × 8 (*Cmcm*-CrB), and 6 × 8 × 6 (*Pnnm*-CrB_4), while for hexagonal lattices the Γ-centered grid was used with *k*-points mesh of 12 × 12 × 12 ($P6/mmm$-CrB_2), 12 × 12 × 12 ($P\bar{6}m2$-CrN), 8 × 8 × 4 ($P6_3/mmc$-Cr_2N), and 8 × 8 × 6 (*R*3*c*-CrN_4).

The hardness was estimated according to three models: the Lyakhov−Oganov model[3] (H_{LO}), Gao's model[90] (H_G), and Chen's model[59] (H_C); in the latter, hardness is calculated using the following relation

$$H_C = 2(k^2G)^{0.585} - 3$$

where k is the Pugh ratio ($k = G/B$), G is the shear modulus, and B is the bulk modulus. The bulk and shear moduli were calculated from the elastic tensors via Voigt−Reuss−Hill (VRH) averaging.[41]

Phase diagrams were obtained using the computed Gibbs free energies G of the relevant phases in the quasiharmonic approximation[91]

$$G(P, T) = E_0(V) + F_{vib}(T, V) + P(T, V)V$$

where E_0 is the total energy from the DFT calculations and F_{vib} is vibrational Helmholtz free energy calculated from the following relation

$$F_{vib}(T, V) = k_BT \int_\Omega g(\omega(V)) \ln\left[1 - \exp\left(-\frac{\hbar\omega(V)}{k_BT}\right)\right] d\omega + \frac{1}{2}\int g(\omega(V))\hbar\omega \, d\omega$$

and the pressure is

$$P(T, V) = -\frac{\partial(E_0(V) + F_{vib}(T, V))}{\partial V}$$

Here $g(\omega(V))$ is the phonon density of states at a given volume, calculated using the finite-displacements approach, where forces on atoms were calculated the VASP package,[84−86] and the phonon frequencies were calculated from the force constants using the PHONOPY package.[92,93] Once Gibbs free energies are computed, phase equilibrium lines on the phase diagram are determined as loci of points where free energies of phases are equal. The chosen approach was validated by a number of reference papers[91,94−99] which calculated the phase diagram $P(T)$ of various materials. Images of crystal structures of the predicted phases were generated using VESTA software.[100]

■ ASSOCIATED CONTENT

Supporting Information

The Supporting Information is available free of charge on the ACS Publications website at DOI: 10.1021/acs.jpclett.6b02821.

Detailed description of the mechanism of the phase transition of CrN from a NaCl-type to WC-type structure, details of calculations of the Cr−N system with the DFT+*U* approach, calculated elastic tensor of studied Cr−C, Cr−B, and Cr−N phases compared with reference data, and electronic properties of Cr−N phases (PDF)

■ AUTHOR INFORMATION

Corresponding Author

*E-mail: A.Kvashnin@skoltech.ru.

ORCID

Alexander G. Kvashnin: 0000-0002-0718-6691

DOI: 10.1021/acs.jpclett.6b02821
J. Phys. Chem. Lett. 2017, 8, 755−764

Notes

The authors declare no competing financial interest.

■ ACKNOWLEDGMENTS

The work was supported by Russian Science Foundation (No. 16-13-10459). Calculations were performed on the Rurik supercomputer at MIPT. The authors thank Prof. Vladislav A. Blatov for help in the application of the TOPOS package for design of the initial transition pathway in CrN (see the Supporting Information).

■ REFERENCES

(1) Liu, A. Y.; Cohen, M. L. Prediction of New Low Compressibility Solids. *Science* **1989**, *245*, 841−842.
(2) Niu, C.; Lu, Y. Z.; Lieber, C. M. Experimental Realization of the Covalent Solid Carbon Nitride. *Science* **1993**, *261*, 334−337.
(3) Lyakhov, A. O.; Oganov, A. R. Evolutionary Search for Novel Superhard Materials: Methodology and Applications to Forms of Carbon and TiO_2. *Phys. Rev. B: Condens. Matter Mater. Phys.* **2011**, *84*, 92103.
(4) Niu, H.; Wang, J.; Chen, X.-Q.; Li, D.; Li, Y.; Lazar, P.; Podloucky, R.; Kolmogorov, A. N. Structure, Bonding, and Possible Superhardness of CrB_4. *Phys. Rev. B: Condens. Matter Mater. Phys.* **2012**, *85*, 144116.
(5) Zhong, M.-M.; Huang, C.; Tian, C.-L. The Structural Stabilities, Mechanical Properties and Hardness of Chromium Tetraboride: Compared with Low-B Borides. *Int. J. Mod. Phys. B* **2016**, *30*, 1650201.
(6) Zhao, Z.; Bao, K.; Tian, F.; Duan, D.; Liu, B.; Cui, T. Potentially Superhard Hcp CrN_2 Compound Studied at High Pressure. *Phys. Rev. B: Condens. Matter Mater. Phys.* **2016**, *93*, 214104.
(7) Pearson, W. B. Chapter XI - An Alphabetical Index of Work on Metals and Alloys. *A Handbook of Lattice Spacings and Structures of Metals and Alloys*; International Series of Monographs on Metal Physics and Physical Metallurgy; Pergamon, 1958; Vol. *4*, pp 254−894.
(8) Loubière, S.; Laurent, C.; Bonino, J. P.; Rousset, A. Elaboration, Microstructure and Reactivity of Cr_3C_2 Powders of Different Morphology. *Mater. Res. Bull.* **1995**, *30*, 1535−1546.
(9) Berg, G.; Friedrich, C.; Broszeit, E.; Berger, C. Development of Chromium Nitride Coatings Substituting Titanium Nitride. *Surf. Coat. Technol.* **1996**, *86−87*, 184−191.
(10) Navinšek, B.; Panjan, P.; Milošev, I. Industrial Applications of CrN (PVD) Coatings, Deposited at High and Low Temperatures. *Surf. Coat. Technol.* **1997**, *97*, 182−191.
(11) Mayrhofer, P. H.; Willmann, H.; Mitterer, C. Oxidation Kinetics of Sputtered Cr−N Hard Coatings. *Surf. Coat. Technol.* **2001**, *146−147*, 222−228.
(12) Čekada, M.; Panjan, P.; Maček, M.; Šmíd, P. Comparison of Structural and Chemical Properties of Cr-Based Hard Coatings. *Surf. Coat. Technol.* **2002**, *151−152*, 31−35.
(13) Kok, Y. N.; Hovsepian, P. E. Resistance of Nanoscale Multilayer C/Cr Coatings against Environmental Attack. *Surf. Coat. Technol.* **2006**, *201*, 3596−3605.
(14) Cheng, F.; Wang, Y.; Yang, T. Microstructure and Wear Properties of Fe−VC−Cr_7C_3 Composite Coating on Surface of Cast Steel. *Mater. Charact.* **2008**, *59*, 488−492.
(15) Vetter, J. Vacuum Arc Coatings for Tools: Potential and Application. *Surf. Coat. Technol.* **1995**, *76−77*, 719−724.
(16) Reiter, A. E.; Derflinger, V. H.; Hanselmann, B.; Bachmann, T.; Sartory, B. Investigation of the Properties of $Al_{1-x}Cr_xN$ Coatings Prepared by Cathodic Arc Evaporation. *Surf. Coat. Technol.* **2005**, *200*, 2114−2122.
(17) Post, B.; Glaser, F. W.; Moskowitz, D. Transition Metal Diborides. *Acta Metall.* **1954**, *2*, 20−25.
(18) Lundström, T. Transition Metal Borides. In *Boron and Refractory Borides*; Matkovich, D. V. I., Ed.; Springer: Berlin, Heidelberg, Germany, 1977; pp 351−376.
(19) Samsonov, G. V.; Vinitskii, I. M. *Handbook of Refractory Compounds* **1980**, 182.
(20) Knappschneider, A.; Litterscheid, C.; Dzivenko, D.; Kurzman, J. A.; Seshadri, R.; Wagner, N.; Beck, J.; Riedel, R.; Albert, B. Possible Superhardness of CrB_4. *Inorg. Chem.* **2013**, *52*, 540−542.
(21) Han, L.; Wang, S.; Zhu, J.; Han, S.; Li, W.; Chen, B.; Wang, X.; Yu, X.; Liu, B.; Zhang, R.; et al. Hardness, Elastic, and Electronic Properties of Chromium Monoboride. *Appl. Phys. Lett.* **2015**, *106*, 221902.
(22) Zhang, R. F.; Wen, X. D.; Legut, D.; Fu, Z. H.; Veprek, S.; Zurek, E.; Mao, H. K. Crystal Field Splitting Is Limiting the Stability and Strength of Ultra-Incompressible Orthorhombic Transition Metal Tetraborides. *Sci. Rep.* **2016**, *6*, 23088.
(23) Okada, S.; Shishido, T.; Yubuta, K.; Mori, T. Synthesis and Some Properties of a New Chromium Boride Cr_2B_3. *Pac. Sci. Rev.* **2012**, *14*, 97−102.
(24) Wang, S.; Yu, X.; Zhang, J.; Zhang, Y.; Wang, L.; Leinenweber, K.; Xu, H.; Popov, D.; Park, C.; Yang, W.; et al. Crystal Structures, Elastic Properties, and Hardness of High-Pressure Synthesized CrB_2 and CrB_4. *J. Superhard Mater.* **2014**, *36*, 279−287.
(25) Coltters, R. G.; Belton, G. R. High Temperature Thermodynamic Properties of the Chromium Carbides Cr_7C_3 and Cr_3C_2 Determined Using a Galvanic Cell Technique. *Metall. Trans. B* **1984**, *15*, 517−521.
(26) Xie, J. Y.; Chen, N. X.; Teng, L. D.; Seetharaman, S. Atomistic Study on the Site Preference and Thermodynamic Properties for $Cr_{23-x}Fe_xC_6$. *Acta Mater.* **2005**, *53*, 5305−5312.
(27) Inoue, A.; Masumoto, T. Formation of Nonequilibrium Cr_3C Carbide in Cr−C Binary Alloys Quenched Rapidly from the Melt. *Scr. Metall.* **1979**, *13*, 711−715.
(28) Liu, B. X.; Cheng, X. Y. A Metastable Cr Carbide of NaCl Structure Formed by Carbon-Ion Implantation into Chromium Films. *J. Phys.: Condens. Matter* **1992**, *4*, L265.
(29) Uebing, C.; Scheuch, V.; Kiskinova, M.; Bonzel, H. P. Segregation of Ordered CrN and CrC Surface Phases on a Fe-15% Cr(100) Crystal. *Surf. Sci.* **1994**, *321*, 89−99.
(30) Andersson, J.-O. A Thermodynamic Evaluation of the Fe-Cr-C System. *Metall. Trans. A* **1988**, *19*, 627−636.
(31) Šimůnek, A. How to Estimate Hardness of Crystals on a Pocket Calculator. *Phys. Rev. B: Condens. Matter Mater. Phys.* **2007**, *75*, 172108.
(32) Li, Y.; Gao, Y.; Xiao, B.; Min, T.; Yang, Y.; Ma, S.; Yi, D. The Electronic, Mechanical Properties and Theoretical Hardness of Chromium Carbides by First-Principles Calculations. *J. Alloys Compd.* **2011**, *509*, 5242−5249.
(33) Jellad, A.; Labdi, S.; Benameur, T. On the Hardness and the Inherent Ductility of Chromium Carbide Nanostructured Coatings Prepared by RF Sputtering. *J. Alloys Compd.* **2009**, *483*, 464−467.
(34) Motono, H.; Yoshinaka, M.; Hirota, K.; Yamaguchi, O. Simultaneous Synthesis and Sintering of Chromium Carbide (Cr_7C_3) Powder by Spark Plasma Sintering Method. *Funtai oyobi Funmatsu Yakin* **2003**, *50*, 372−376.
(35) Esteve, J.; Romero, J.; Gómez, M.; Lousa, A. Cathodic Chromium Carbide Coatings for Molding Die Applications. *Surf. Coat. Technol.* **2004**, *188−189*, 506−510.
(36) Hasegawa, M.; Yagi, T. Systematic Study of Formation and Crystal Structure of 3d-Transition Metal Nitrides Synthesized in a Supercritical Nitrogen Fluid under 10 GPa and 1800 K Using Diamond Anvil Cell and YAG Laser Heating. *J. Alloys Compd.* **2005**, *403*, 131−142.
(37) Rivadulla, F.; Bañobre-López, M.; Quintela, C. X.; Piñeiro, A.; Pardo, V.; Baldomir, D.; López-Quintela, M. A.; Rivas, J.; Ramos, C. A.; Salva, H.; et al. Reduction of the Bulk Modulus at High Pressure in CrN. *Nat. Mater.* **2009**, *8*, 947−951.
(38) Corliss, L. M.; Elliott, N.; Hastings, J. M. Antiferromagnetic Structure of CrN. *Phys. Rev.* **1960**, *117*, 929−935.
(39) Wang, S.; Yu, X.; Zhang, J.; Chen, M.; Zhu, J.; Wang, L.; He, D.; Lin, Z.; Zhang, R.; Leinenweber, K.; et al. Experimental Invalidation of

DOI: 10.1021/acs.jpclett.6b02821
J. Phys. Chem. Lett. 2017, 8, 755−764

Phase-Transition-Induced Elastic Softening in CrN. *Phys. Rev. B: Condens. Matter Mater. Phys.* **2012**, *86*, 64111.
(40) Zhang, X. Y.; Chawla, J. S.; Deng, R. P.; Gall, D. Epitaxial Suppression of the Metal-Insulator Transition in CrN. *Phys. Rev. B: Condens. Matter Mater. Phys.* **2011**, *84*, 73101.
(41) Filippetti, A.; Hill, N. A. Magnetic Stress as a Driving Force of Structural Distortions: The Case of CrN. *Phys. Rev. Lett.* **2000**, *85*, 5166−5169.
(42) Alling, B.; Marten, T.; Abrikosov, I. A. Questionable Collapse of the Bulk Modulus in CrN. *Nat. Mater.* **2010**, *9*, 283−284.
(43) Herwadkar, A.; Lambrecht, W. R. L. Electronic Structure of CrN: A Borderline Mott Insulator. *Phys. Rev. B: Condens. Matter Mater. Phys.* **2009**, *79*, 35125.
(44) Alling, B.; Marten, T.; Abrikosov, I. A. Effect of Magnetic Disorder and Strong Electron Correlations on the Thermodynamics of CrN. *Phys. Rev. B: Condens. Matter Mater. Phys.* **2010**, *82*, 184430.
(45) Hones, P.; Sanjines, R.; Levy, F. Characterization of Sputter-Deposited Chromium Nitride Thin Films for Hard Coatings. *Surf. Coat. Technol.* **1997**, *94*−*95*, 398−402.
(46) Tricoteaux, A.; Jouan, P. Y.; Guerin, J. D.; Martinez, J.; Djouadi, A. Fretting Wear Properties of CrN and Cr_2N Coatings. *Surf. Coat. Technol.* **2003**, *174*−*175*, 440−443.
(47) Lin, J.; Sproul, W. D.; Moore, J. J.; Lee, S.; Myers, S. High Rate Deposition of Thick CrN and Cr_2N Coatings Using Modulated Pulse Power (MPP) Magnetron Sputtering. *Surf. Coat. Technol.* **2011**, *205*, 3226−3234.
(48) Qi, Z. B.; Liu, B.; Wu, Z. T.; Zhu, F. P.; Wang, Z. C.; Wu, C. H. A Comparative Study of the Oxidation Behavior of Cr_2N and CrN Coatings. *Thin Solid Films* **2013**, *544*, 515−520.
(49) Aguas, M. D.; Nartowski, A. M.; Parkin, I. P.; MacKenzie, M.; Craven, A. J. Chromium Nitrides (CrN, Cr_2N) from Solid State Metathesis Reactions: Effects of Dilution and Nitriding Reagent. *J. Mater. Chem.* **1998**, *8*, 1875−1880.
(50) Eriksson, S. X-Ray Investigation of the System Iron-Chromium-Nitrogen. *Jernkont. Ann.* **1934**, *118*, 530−543.
(51) Shah, H. N.; Jayaganthan, R.; Kaur, D.; Chandra, R. Influence of Sputtering Parameters and Nitrogen on the Microstructure of Chromium Nitride Thin Films Deposited on Steel Substrate by Direct-Current Reactive Magnetron Sputtering. *Thin Solid Films* **2010**, *518*, 5762−5768.
(52) Cecchini, R.; Fabrizi, A.; Cabibbo, M.; Paternoster, C.; Mavrin, B. N.; Denisov, V. N.; Novikova, N. N.; Haïdopoulo, M. Mechanical, Microstructural and Oxidation Properties of Reactively Sputtered Thin CrN Coatings on Steel. *Thin Solid Films* **2011**, *519*, 6515−6521.
(53) Kim, S.-J.; Marquart, T.; Franzen, H. F. Structure Refinement for Cr_2N. *J. Less-Common Met.* **1990**, *158*, L9−L10.
(54) Yan, M. F.; Chen, H. T. Structural, Elastic and Electronic Properties of Cr_2N: A First-Principles Study. *Comput. Mater. Sci.* **2014**, *88*, 81−85.
(55) Okada, S.; Kudou, K.; Iizumi, K.; Kudaka, K.; Higashi, I.; Lundström, T. Single-Crystal Growth and Properties of CrB, Cr_3B_4, Cr_2B_3 and CrB_2 from High-Temperature Aluminum Solutions. *J. Cryst. Growth* **1996**, *166*, 429−435.
(56) Jiang, C. First-Principles Study of Structural, Elastic, and Electronic Properties of Chromium Carbides. *Appl. Phys. Lett.* **2008**, *92*, 041909.
(57) Xiao, B.; Xing, J. D.; Feng, J.; Li, Y. F.; Zhou, C. T.; Su, W.; Xie, X. J.; Chen, Y. H. Theoretical Study on the Stability and Mechanical Property of Cr_7C_3. *Phys. B* **2008**, *403*, 2273−2281.
(58) Yakel, H. L. Atom Distributions in Tau-Carbide Phases: Fe and Cr Distributions in $(Cr_{23-X}Fe_X)C_6$ with X = 0, 0.7$_4$, 1.7$_0$, 4.1$_3$ and 7.3$_6$. *Acta Crystallogr., Sect. B: Struct. Sci.* **1987**, *43*, 230−238.
(59) Chen, X.-Q.; Niu, H.; Li, D.; Li, Y. Modeling Hardness of Polycrystalline Materials and Bulk Metallic Glasses. *Intermetallics* **2011**, *19*, 1275−1281.
(60) Fahy, S.; Louie, S. G.; Cohen, M. L. Pseudopotential Total-Energy Study of the Transition from Rhombohedral Graphite to Diamond. *Phys. Rev. B: Condens. Matter Mater. Phys.* **1986**, *34*, 1191−1199.
(61) Furthmüller, J.; Hafner, J.; Kresse, G. Ab Initio Calculation of the Structural and Electronic Properties of Carbon and Boron Nitride Using Ultrasoft Pseudopotentials. *Phys. Rev. B: Condens. Matter Mater. Phys.* **1994**, *50*, 15606−15622.
(62) Haines, J.; Léger, J. M.; Bocquillon, G. Synthesis and Design of Superhard Materials. *Annu. Rev. Mater. Res.* **2001**, *31*, 1−23.
(63) Hirota, K.; Mitani, K.; Yoshinaka, M.; Yamaguchi, O. Simultaneous Synthesis and Consolidation of Chromium Carbides (Cr_3C_2, Cr_7C_3 and $Cr_{23}C_6$) by Pulsed Electric-Current Pressure Sintering. *Mater. Sci. Eng., A* **2005**, *399*, 154−160.
(64) Xiao, B.; Feng, J.; Zhou, C. T.; Xing, J. D.; Xie, X. J.; Chen, Y. H. First Principles Study on the Electronic Structures and Stability of Cr_7C_3 Type Multi-Component Carbides. *Chem. Phys. Lett.* **2008**, *459*, 129−132.
(65) Yu, H.; Duan, D.; Tian, F.; Liu, H.; Li, D.; Huang, X.; Liu, Y.; Liu, B.; Cui, T. Polymerization of Nitrogen in Ammonium Azide at High Pressures. *J. Phys. Chem. C* **2015**, *119*, 25268−25272.
(66) Popov, M. Raman and IR Study of High-Pressure Atomic Phase of Nitrogen. *Phys. Lett. A* **2005**, *334*, 317−325.
(67) Müller, U. *Inorganic Structural Chemistry*; John Wiley & Sons, 2007.
(68) Stishov, S. M.; Popova, S. V. A New Dense Modification of Silica. *Geochem* **1961**, *10*, 923−926.
(69) Novoselov, K. S.; Jiang, D.; Schedin, F.; Booth, T. J.; Khotkevich, V. V.; Morozov, S. V.; Geim, A. K. Two-Dimensional Atomic Crystals. *Proc. Natl. Acad. Sci. U. S. A.* **2005**, *102*, 10451−10453.
(70) Clark, K. W.; Qin, S.; Zhang, X.-G.; Li, A.-P. Nanoscale Periodic Modulations on Sodium Chloride Surface Revealed by Tuning Fork Atomic Force Microscopy. *Nanotechnology* **2012**, *23*, 185306.
(71) Qian, G.-R.; Dong, X.; Zhou, X.-F.; Tian, Y.; Oganov, A. R.; Wang, H.-T. Variable Cell Nudged Elastic Band Method for Studying Solid−solid Structural Phase Transitions. *Comput. Phys. Commun.* **2013**, *184*, 2111−2118.
(72) Kinney, G. F.; Graham, K. J. *Explosive Shocks in Air*; Springer Science & Business Media: New York, 1985.
(73) O'Neil, M. J. *The Merck Index - An Encyclopedia of Chemicals, Drugs, and Biologicals*; Merck and Co., Inc., Whitehouse Station, NJ, 2001.
(74) Asay, B. *Shock Wave Science and Technology Reference Library*, 1st ed.; Springer-Verlag: Berlin, Heidelberg, Germany, 2010; Vol. *5*.
(75) Oganov, A. R.; Glass, C. W. Crystal Structure Prediction Using Ab Initio Evolutionary Techniques: Principles and Applications. *J. Chem. Phys.* **2006**, *124*, 244704.
(76) Oganov, A. R.; et al. Evolutionary Crystal Structure Prediction as a Method for the Discovery of Minerals and Materials. *Rev. Mineral. Geochem.* **2010**, *71*, 271.
(77) Oganov, A. R.; Lyakhov, A. O.; Valle, M. How Evolutionary Crystal Structure Prediction Works—and Why. *Acc. Chem. Res.* **2011**, *44*, 227−237.
(78) Lyakhov, A. O.; Oganov, A. R.; Valle, M. How to Predict Very Large and Complex Crystal Structures. *Comput. Phys. Commun.* **2010**, *181*, 1623−1632.
(79) Lyakhov, A. O.; Oganov, A. R.; Stokes, H. T.; Zhu, Q. New Developments in Evolutionary Structure Prediction Algorithm USPEX. *Comput. Phys. Commun.* **2013**, *184*, 1172−1182.
(80) Glass, C. W.; Oganov, A. R.; Hansen, N. USPEX—Evolutionary Crystal Structure Prediction. *Comput. Phys. Commun.* **2006**, *175*, 713−720.
(81) Hohenberg, P.; Kohn, W. Inhomogeneous Electron Gas. *Phys. Rev.* **1964**, *136* (3B), B864−B871.
(82) Kohn, W.; Sham, L. J. Self-Consistent Equations Including Exchange and Correlation Effects. *Phys. Rev.* **1965**, *140* (4), A1133−A1138.
(83) Perdew, J. P.; Burke, K.; Ernzerhof, M. Generalized Gradient Approximation Made Simple. *Phys. Rev. Lett.* **1996**, *77* (18), 3865−3868.

DOI: 10.1021/acs.jpclett.6b02821
J. Phys. Chem. Lett. 2017, 8, 755−764

(84) Kresse, G.; Hafner, J. Ab Initio Molecular Dynamics for Liquid Metals. *Phys. Rev. B: Condens. Matter Mater. Phys.* **1993**, *47* (1), 558−561.
(85) Kresse, G.; Hafner, J. Ab Initio Molecular-Dynamics Simulation of the Liquid-Metal-Amorphous-Semiconductor Transition in Germanium. *Phys. Rev. B: Condens. Matter Mater. Phys.* **1994**, *49* (20), 14251−14269.
(86) Kresse, G.; Furthmüller, J. Efficient Iterative Schemes for Ab Initio Total-Energy Calculations Using a Plane-Wave Basis Set. *Phys. Rev. B: Condens. Matter Mater. Phys.* **1996**, *54* (16), 11169−11186.
(87) Anisimov, V. I.; Zaanen, J.; Andersen, O. K. Band Theory and Mott Insulators: Hubbard U instead of Stoner I. *Phys. Rev. B: Condens. Matter Mater. Phys.* **1991**, *44*, 943−954.
(88) Dudarev, S. L.; Botton, G. A.; Savrasov, S. Y.; Humphreys, C. J.; Sutton, A. P. Electron-Energy-Loss Spectra and the Structural Stability of Nickel Oxide: An LSDA+U Study. *Phys. Rev. B: Condens. Matter Mater. Phys.* **1998**, *57*, 1505−1509.
(89) Monkhorst, H. J.; Pack, J. D. Special Points for Brillouin-Zone Integrations. *Phys. Rev. B* **1976**, *13* (12), 5188−5192.
(90) Gao, F.; He, J.; Wu, E.; Liu, S.; Yu, D.; Li, D.; Zhang, S.; Tian, Y. Hardness of Covalent Crystals. *Phys. Rev. Lett.* **2003**, *91*, 015502−015506.
(91) Kern, G.; Kresse, G.; Hafner, J. Ab Initio Calculation of the Lattice Dynamics and Phase Diagram of Boron Nitride. *Phys. Rev. B: Condens. Matter Mater. Phys.* **1999**, *59*, 8551−8559.
(92) Togo, A.; Tanaka, I. First Principles Phonon Calculations in Materials Science. *Scr. Mater.* **2015**, *108*, 1−5.
(93) Togo, A.; Oba, F.; Tanaka, I. First-Principles Calculations of the Ferroelastic Transition between Rutile-Type and $CaCl_2$-Type SiO_2 at High Pressures. *Phys. Rev. B: Condens. Matter Mater. Phys.* **2008**, *78*, 134106.
(94) Luo, W.; Windl, W. First Principles Study of the Structure and Stability of Carbynes. *Carbon* **2009**, *47*, 367−383.
(95) Kvashnin, A. G.; Chernozatonskii, L. A.; Yakobson, B. I.; Sorokin, P. B. Phase Diagram of Quasi-Two-Dimensional Carbon, From Graphene to Diamond. *Nano Lett.* **2014**, *14*, 676−681.
(96) Kvashnin, A. G.; Sorokin, P. B. Lonsdaleite Films with Nanometer Thickness. *J. Phys. Chem. Lett.* **2014**, *5*, 541−548.
(97) Oganov, A. R.; Gillan, M. J.; Price, G. D. Ab Initio Lattice Dynamics and Structural Stability of MgO. *J. Chem. Phys.* **2003**, *118*, 10174−10182.
(98) Oganov, A. R.; Gillan, M. J.; Price, G. D. Structural Stability of Silica at High Pressures and Temperatures. *Phys. Rev. B: Condens. Matter Mater. Phys.* **2005**, *71*, 64104.
(99) Oganov, A. R.; Ono, S. Theoretical and Experimental Evidence for a Post-Perovskite Phase of $MgSiO_3$ in Earth's D' Layer. *Nature* **2004**, *430*, 445−448.
(100) Momma, K.; Izumi, F. VESTA 3 for Three-Dimensional Visualization of Crystal, Volumetric and Morphology Data. *J. Appl. Crystallogr.* **2011**, *44*, 1272−1276.

NOTE ADDED IN PROOF

Just before the publication of this paper, our other paper (Zhang, J.; Oganov, A. R.; Li, X.; Niu, H. Pressure-stabilized hafnium nitrides and their properties. *Phys. Rev. B* **2016** *95*, 0201 03(R)) appeared, predicting a very interesting high-energy-density phase HfN_{10} at pressures above 23 GPa; its structure also features polymeric nitrogen chains.

NOTE ADDED AFTER ASAP PUBLICATION

This paper was published ASAP on January 31, 2017. Text was updated. The revised paper was reposted on February 3, 2017.

DOI: 10.1021/acs.jpclett.6b02821
J. Phys. Chem. Lett. 2017, 8, 755−764